

Article

Effect of Magnesium Hydroxide and Aluminum Hydroxide as Thermal Barriers on the Flame-Retardant Behavior of Acrylic-Based Coating

Giuseppe Scionti ¹, Elpida Piperopoulos ^{1,*}, Mario Atria ², Luigi Calabrese ¹ and Edoardo Proverbio ¹

¹ Dipartimento di Ingegneria, Università di Messina, Contrada di Dio- Sant'Agata, 98166 Messina, Italy; pepi_scionti@hotmail.com (G.S.); lcalabrese@unime.it (L.C.); eproverbio@unime.it (E.P.)

² Colorificio Atria, Contrada Camarro Formeca, 91028 Partanna, Italy; amario@atria.it

* Correspondence: epiperopoulos@unime.it

Abstract: In the effort to improve fire safety in residential, industrial, or naval structures, the study of flame-retardant coatings has become increasingly interesting. Flame-retardant additives are definitely the most traveled route; however, often these additives are halogenated compounds that increase the amount of smoke and toxic decomposition of the products during polymer combustion. It is necessary to develop new fire retardant (FR) agents that respect the environment and are safe for human health. This work aims to study two completely harmless hydroxides, Mg(OH)₂ and Al(OH)₃, added in low percentages (2 wt.%) to an already marketed acrylic polymer emulsion (79.2 wt.% of solid content, 37.3 wt.% and 41.8 wt.%, respectively, for polymer and fillers contents) in order to decrease the dangerous effects of these additives on the physical integrity and durability of the coatings. The hydroxides content was added in 6.2 wt.% and 5.6 wt.%, respectively, to polymer and total solids present in the emulsion. Flame exposure tests are conducted at different times (15 s and 30 s) to verify the flame stability and thermal insulation exerted by the investigated coatings. Furthermore, through a precise analysis of the areas damaged by the combustion process, it is possible to link the flame-retardant properties to the FR choice and its particle size, finding a promising solution in the sample based on small Mg(OH)₂ particles for fire protection in naval applications.

Keywords: thermal barrier filler; flame-retardant coating; magnesium hydroxide; aluminum hydroxide



Citation: Scionti, G.; Piperopoulos, E.; Atria, M.; Calabrese, L.; Proverbio, E. Effect of Magnesium Hydroxide and Aluminum Hydroxide as Thermal Barriers on the Flame-Retardant Behavior of Acrylic-Based Coating. *Coatings* **2023**, *13*, 1517. <https://doi.org/10.3390/coatings13091517>

Academic Editors: Ivan Jerman, Lukasz Gierz, Mariola Robakowska and Paulina Paulina Mayer

Received: 20 July 2023

Revised: 17 August 2023

Accepted: 25 August 2023

Published: 28 August 2023



Copyright: © 2023 by the authors. Licensee MDPI, Basel, Switzerland. This article is an open access article distributed under the terms and conditions of the Creative Commons Attribution (CC BY) license (<https://creativecommons.org/licenses/by/4.0/>).

1. Introduction

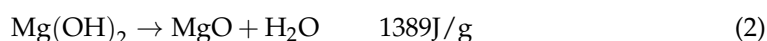
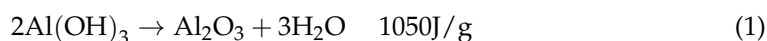
Flame-retardant coatings are a relevant research field of fire safety, providing protection for residential or industrial infrastructure [1]. These coatings act by avoiding or reducing the spread of fire and heat, thereby reducing accidental damage risks to structures and human health [2].

A novel method for enhancing the ability of composite coatings to resist flames involves integrating flame retardant additives into their composition. [3]. These particles can be added to coatings to improve their efficiency, providing beneficial effects on durability in critical environmental conditions [4].

However, an important aspect that needs to be considered in the development of flame-retardant coatings is the identification of unarmful additives, which can allow a further benefit in the reduction of the environmental impact induced by the proposed solution. Several traditional thermal barrier coatings contain toxic chemicals that negatively affect the coating's sustainability [5,6]; therefore, ongoing research and development are essential to ensure that they remain effective and environmentally friendly. In this concern, new eco-friendly flame retardant (FR) compounds could be identified as promising additives for fire retardant composite coatings, free from harmful chemicals.

Magnesium hydroxide and aluminum hydroxide are two nontoxic and environmentally friendly options suitably applied in recent years, due to their effectiveness in reducing

smoke and toxic fumes during a fire. These materials are abundant, inexpensive, and do not contain halogen or heavy metals, which can be harmful to human health and the environment. Their flame-retardant behavior is supplied by releasing water vapor absorbing energy in their dehydration process and hereby limiting the thermal flow during direct flame exposure [7]. In particular, the involved decomposition reaction of both FR hydroxides are detailed below [8,9]:



Both dehydration reactions are characterized by a high heat of reaction. Therefore, the triggering of these endothermic reactions permits a large heat dissipation during a direct flame impingement, implying a cooling effect on the polymer-based coating. In addition, the water vapor produced during the dehydration reaction can both dilute the flammable gas (hindering the combustion growth), absorb smoke particles (limiting the smoke formation), cool the surface, and form a protective layer of stable aluminum oxide or magnesium oxide. These fillers can be incorporated into coatings as a powder, or as a predispersed slurry, and can be used in various types of coatings, including water-based, solvent-based, and powder coatings. However, in order to achieve these flame-retardant specific capabilities, a high filler content is required, usually greater than 60% by weight (37% by volume) in polymer matrices, which results in a significant loss of mechanical performance in the coating [7].

Different studies have shown that the addition of $\text{Mg}(\text{OH})_2$ and $\text{Al}(\text{OH})_3$ fillers are able to significantly improve the flame retardant features of coatings, leading to a decrease in the heat release rate, smoke production, and an increase in the ignition time of the composite coating [10–12].

Several studies assessed the efficiency of $\text{Mg}(\text{OH})_2$ and $\text{Al}(\text{OH})_3$ compounds as FR fillers in composite materials coatings. Yew et al. [13] investigated the effect of the combination of acrylic binder and flame-retardant ingredients (aluminum hydroxide ($\text{Al}(\text{OH})_3$) and titanium dioxide (TiO_2)) for fire protective solvent-based coatings optimized for steel substrates. It was observed that the combination of $\text{Al}(\text{OH})_3$ and TiO_2 significantly improved the fire protection and thermal stability, achieving an LOI value of 34, indicative of a good flame stability.

Liang et al. in [14,15] assessed the effect of aluminum hydroxide, magnesium hydroxide and zinc borate in the flame-retardant behavior of a polypropylene based composite coating. The FR fillers content were incorporated in the matrix in a wide range content (10–70 phr). The results evidenced the suitability of $\text{Al}(\text{OH})_3$ and $\text{Mg}(\text{OH})_2$ fillers in the reduction in the flammability and smoke generation of the material. The optimal fire-retardant performances were achieved for the formulation with 70 phr of FR additives.

Similarly, Chen et al. [16] evaluated the synergic effectiveness of cellulose nanocrystals and magnesium hydroxide fillers in polyurethane wood coating, showing a reduction in the flammability, achieving, for $\text{M}(\text{OH})_2 > 40$ wt.%, B1 level (flame-retardant material). Analogous considerations were experienced by Chen et al. [17] by using $\text{Mg}(\text{OH})_2$ as a fire retardant at varying filler content (10–60 wt.%) in the composites, demonstrating a significant improvement in fire performance.

Based on these considerations, $\text{Mg}(\text{OH})_2$ and $\text{Al}(\text{OH})_3$ could play a crucial role in fire safety as prepared composite coatings are becoming even more effective and environmentally friendly as a suitable tool in protecting structure and human health. However, both compounds have their advantages and disadvantages; therefore, an improvement in knowledge of the choice of which to use during direct flame impingement is a desired outcome for its industrial application.

Nevertheless, high percentages of flame retardants have dangerous effects on the mechanical stability and durability of the coating. In creating fire-resistant composite coatings, it is essential to intricately design and maintain a harmonious balance between

their mechanical characteristics and flame-retardant attributes [18]. Hence, the investigation for coating formulations characterized by lower flame-retardant contents can be considered a successful approach to attain an effective tailoring both of mechanical stability and fire-retardant performances. In this sense, the development of a low FR loaded systems that combine active and passive fire protection could be a promising strategy to obtain a customized well-structured coating.

In this concern, the aim of this paper is to assess the effect of $\text{Mg}(\text{OH})_2$ and $\text{Al}(\text{OH})_3$ on the flame-retardant behavior of acrylic-based coatings for naval applications. To enhance the fire-retardant behavior and stability of the coatings, low amounts of magnesium hydroxide and aluminum hydroxide fillers were added to FR, to an already marketed formulation. Fillers with different particle size and morphology were incorporated into the acrylic polymeric matrix. A reaction-to-fire test adapted from EN ISO 11925-2 was performed at two different direct fire exposure times (15 and 30 s) to assess the flame-retardant behavior of the proposed formulations.

2. Materials and Methods

2.1. Materials

Two kinds of fillers, aluminum hydroxide ($\text{Al}(\text{OH})_3$) and magnesium hydroxide ($\text{Mg}(\text{OH})_2$) were used as fire retardant (FR) fillers to improve the flame-retardant behavior of an acrylic based coating. Furthermore, to better assess the effect of the FR particle size on the coating's fire-retardant performance, commercial and laboratory synthesized FR fillers were employed. The commercial aluminum hydroxide, $\text{Al}(\text{OH})_3$ (coded C-AH), was purchased from Sigma Aldrich (reagent grade, St. Louis, MO, USA). The laboratory synthesized one was obtained by precipitation method (coded S-AH). Two commercial magnesium hydroxides, $\text{Mg}(\text{OH})_2$, were purchased from Acros Organics B.V.B.A. (95 wt.%, Waltham, MA, USA) and Kisuma Chemicals BV (>98 wt.%, Veendam, The Netherlands), named C1-MH and C2-MH, respectively. The particle morphology of all FR fillers is shown in Figure 1, detected by Scanning Electron Microscopy (SEM, Quanta 450, FEI, Hillsboro, OR, USA), performed in low vacuum with an accelerating voltage of 20 kV.

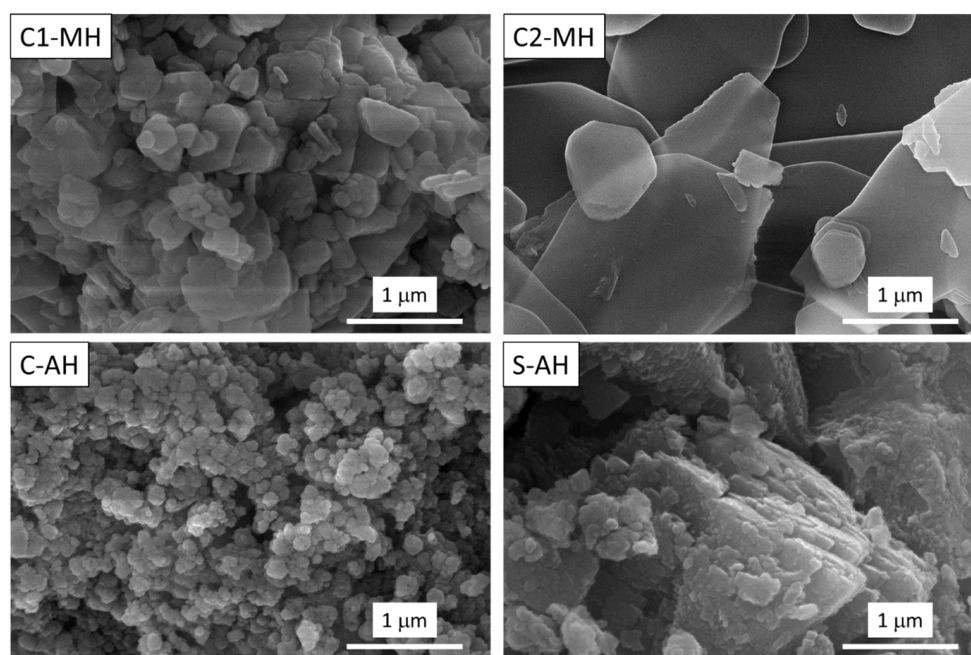


Figure 1. Morphology of the employed FR fillers, C1-MH, C2-MH, C-AH, and S-AH137.

Concerning aluminum hydroxide fillers, C-AH is characterized by a small spherical particle size (average value \sim of 137.5 nm). Instead, S-AH exhibits a wider distribution

in particle size. The shape and dimension of the filler is inhomogeneous and not regular. Furthermore, a packed morphology is also noticed, probably ascribed to a coalescence phenomenon among the material's particles. Concerning magnesium hydroxide fillers, C1-MH is constituted of particles of different size and shape (spheroidal and polygonal), but not packed and clearly distinguishable from each other (average particle size of 284.8 nm). Finally, C2-MH shows a totally different morphology. Plate-like particles, typical of brucite phase [19], randomly packed and dimension mainly in the range 3–5 μm , are observed.

The used reagents were aluminum nitrate hexahydrate, $\text{Al}(\text{NO}_3)_3 \cdot 9\text{H}_2\text{O}$ (99 wt.%, Carlo Erba Reagents, Milan, Italy), and ammonium hydroxide, NH_4OH , (30 wt.%, Honeywell Fluka, Charlotte, NC, USA).

The synthesis was carried out by stirring, adding 50 mL of a 0.9 mol/L NH_4OH solution (pH = 11.8) stepwise to 100 mL of $\text{Al}(\text{NO}_3)_3$, 0.13 mol/L, while stirring (final solution pH = 8.49) using a peristaltic pump (2.5 mL/min) to obtain 3 g of precipitate.

The resulting solution was allowed to stand at room temperature for 24 h before being filtered under vacuum using a 0.22 μm thick filter. The precipitate was then washed with deionized water and dried in an oven at 80 $^\circ\text{C}$ overnight. $\text{Al}(\text{OH})_3$ was used in its purest form.

2.2. Coatings Preparation and Characterization

All coating batches were prepared by Colorificio Atria S.r.l. paint factory (Contrada Cammaro Formeca, Partanna (TP), Italy), adding the previously discussed fillers into an already commercial acrylic formulation used as basic reference. In the basic reference, different conventional additives are present (79.2 wt.% of solid content, 37.3 wt.% and 41.8 wt.%, respectively, for polymer and filler contents), i.e., TiO_2 , CaCO_3 , and hollow glass microspheres (glass HMS, Sarco S.r.l., Marsala (TP), Italia). TiO_2 nanoparticles are used to decrease the flame-spread rate [20]. Calcium carbonate has a role, enhancing the scratch resistance of the coating [21]. Glass HMS are used to decrease the density of the composite coating, to increase temperature insulation, without prejudicing its mechanical stability [22]. All the slurry batches were applied on a stainless steel sheet (dimension 75 mm \times 140 mm \times 0.8 mm) using a BYK manual film applicator (coating thickness 770 μm). All samples were codified using two prefixes: the first one is referred to flame retardant (FR) filler typology. MH and AH are used for magnesium hydroxide and aluminum hydroxide, respectively. The second one is referred to filler particle size (S and L are applied for small and large size of the FR particles). As reference, the batch AH-L is referred to as a coating batch loaded with large-sized particles of aluminum hydroxide filler. Furthermore, the TS code was used to identify the unfilled reference sample. TS coating has the same composition of the investigated samples without adding the $\text{Mg}(\text{OH})_2$ and $\text{Al}(\text{OH})_3$ fillers. Finally, a standard nonflame coating (STD) was, also, identified by Colorificio Atria S.r.l. to better assess the thermal insulation capacity of the flame-retardant modified coatings. STD is a commercial water-based painting (Colorificio Atria S.r.l.), composed of an acrylic binder (20 wt.%), quartz sand (8 wt.%), calcium carbonate (25 wt.%), and antibubble, antifoam, and rheological thickener fillers (1–2 wt.%). Table 1 summarizes codes, and FR compound specifications for all references and FR modified composite coatings.

Table 1. Codes, definition, and FR compound specifications of the composite coatings.

Code	Definition	FR Typology	FR Content (wt.%)	FR Specifications
STD	Nonflame retardant coating	//	//	//
TS	Unfilled flame retardant coating	//	//	//
MH-S	Filled flame retardant coating	$\text{Mg}(\text{OH})_2$	2	Acros Organics—United States
MH-L	Filled flame retardant coating	$\text{Mg}(\text{OH})_2$	2	Kisuma Chemicals BV—The Netherlands
AH-S	Filled flame retardant coating	$\text{Al}(\text{OH})_3$	2	Sigma-Aldrich—United States
AH-L	Filled flame retardant coating	$\text{Al}(\text{OH})_3$	2	Synthesized by precipitation

The structural characterization was performed by a D8 Advanced Bruker diffractometer (Bruker, Billerica, MA, USA) in Bragg–Brentano θ – 2θ configuration, with Cu K α radiation at 40 V and 40 mA. Each scan was acquired in the 2θ range from 10° to 80° with a step size of 0.010° and a counting time of 0.1 s.

2.3. Fire-Retardant Behavior Measurement

The reaction-to-fire test, adapted from EN ISO 119225-2, was carried out on all coated steel batches. During the European ignitability test, a propane gas flame is brought into contact with the product (temperature of 180°C). The flame spread shouldn't reach a height of 15 cm in a certain amount of time. In addition, the occurrence and duration of flaming and glowing are observed. The laboratory test, used in this work, involves the assessment of fire-retardant performance of the coatings (placed in a vertical position) subjected to direct impingement of flame (flame length 20 ± 5 mm, incidence angle $45 \pm 1^\circ$). The test set-up configuration was implemented to record during the ignition and cooling time the sample temperature in the front and back of the sample. In particular, a contact thermocouple was placed on the back of the specimen in order to acquire the temperature evolution on the opposite side to the fire exposure. In addition, a thermal camera was placed to record the temperature evolution and distribution on the front side of the sample. A high-definition camera was also used to monitor visually the reaction to fire of the sample's front.

The experimental set-up of the applied "reaction-to-fire" test is schematized in Figure 2, according to the assembly proposed by [23].

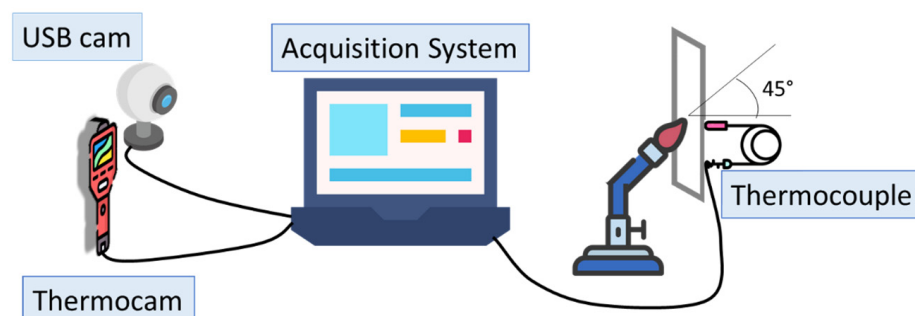


Figure 2. Burning system set-up.

The painted stainless steel samples ($75\text{ mm} \times 140\text{ mm}$) are fixed vertically in a test hood chamber. The center of the surface was exposed to an impingement of flame, supplied by a Bunsen burner (15 and 30 s of direct flame exposition were carried out). Two replicas for each batch were performed.

2.4. Fire-Induced Defect Distribution

With the purpose to correlate the thermal barrier capacity with fire retardant compound and coating batch, a quantitative analysis of the shape and distribution of the fire-induced defects in the coating surface was carried out by means of digital image analysis (DIA) performed on optical images of the degraded samples. The analysis was performed on the whole sample surface. Due to a not monotone contrast of the several defects contour, the DIA was processed by using a semiautomatic procedure. At first, based on experienced images, different color thresholds were identified. Then, an image analysis script written in python (Python 3.10.4) was used to discriminate the amount and the relative shape of the thermally affected zones. All the fire-induced defect data were clustered in classes calculating their number, N_C , and dimensional width, w_C , according to the Sturges rule [24]:

$$N_C = \log_2(N_b) + 1 \quad (3)$$

$$w_C = \frac{A_{max} - A_{min}}{N_C} \quad (4)$$

where N_b is the number of acquired defects, and A_{max} and A_{min} are the areas of the largest and smallest measured defects, respectively.

3. Results and Discussion

3.1. Fire Retardant Performances

Preliminarily, in order to evaluate how the reaction to fire of the coated steel samples evolves during the flame impingement test, Figure 3 shows the evolution of the backside temperature of three types of coatings, a standard coating (STD), which is not flame retardant, and two heat insulating coatings. For this comparison, the magnesium hydroxide (MH-L) and aluminum hydroxide (AH-L) based coatings were considered. Results related to a fire exposure of 15 s and 30 s are, furthermore, compared.

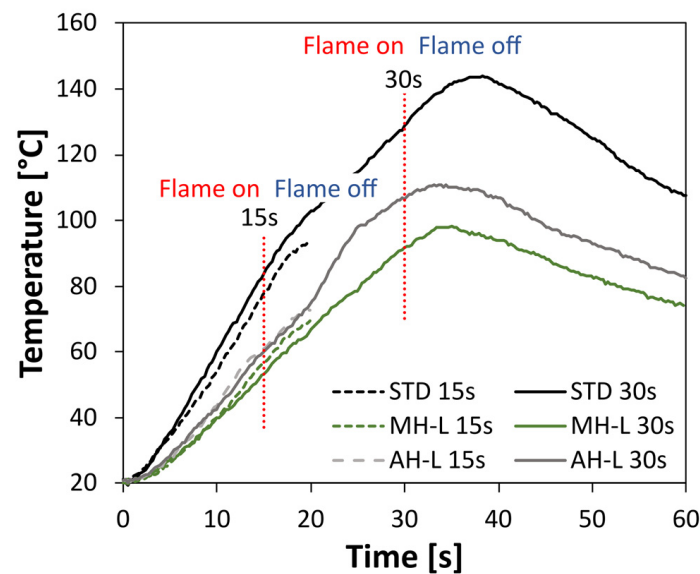


Figure 3. Back temperature evolution on STD, MH-L, and AH-L samples to direct impingement flame (15 s and 30 s).

The STD samples exhibited a relevant sensitivity to the direct flame impingement. At 30 s, the STD coated surface is largely degraded, and the backside temperature (measured by the thermocouple probe) shows a relevant and progressive increase in temperature. In particular, after 15 s and 30 s of flame exposition, the temperature is 83.8 °C and 129.5 °C, respectively.

Further information can be obtained by considering the trend of the curves relating to 15 s and 30 s. The trend is very similar during the flame on phase indicating that the specimens underwent a similar heating condition. A discordant behavior is found at the end of the heating phase (beginning of the flame off phase). After the flame is put out within 15 s, the temperature continues to escalate due to thermal inertia, but doesn't attain a stable state by the end of the 20 s measurement. This indicates that flame retardants might require longer periods of exposure to provide comprehensive protection. The findings imply that brief exposure durations might not suffice to ensure complete defense against fire, and it might be essential to utilize stronger flame-retardant substances for the best possible fire safety. The STD 30 s sample has a maximum temperature equal to 143.7 °C at 37 s. Subsequently, the specimen is cooled with a progressive reduction in the temperature. However, after 60 s (30 s after the flame goes out), the backside temperature of the sample is still 107.5 °C. This settles that the fire barrier capability guaranteed by the STD coating is quite limited. The coating does not supply a protection against the thermal flux imposed

during the direct flame impingement. Consequently, the choice of adding thermally active particles represents a potentially effective approach to increase the flame stability and protection of the composite coating under direct exposure to fire service conditions.

The MH-L sample showed a more effective reaction to fire and flame stability than the STD one. Evaluating the evolution of the temperature over time, it can be seen that the coating treated with FR filler has a better heat barrier action, which can be seen from the lower temperature reached throughout the test time. In particular, after 15 s and 30 s of direct flame exposure, the temperature on the rear side of the sample is 54.1 °C and 91.8 °C, respectively. These values are approximately 30–40 °C lower than the STD sample. These findings suggest that the heat transfer, facilitated by the heat dispersion caused by magnesium hydroxide, is significantly restricted, leading to positive impacts on the coating's resistance to flames. The AH-L batch exhibits an intermediate trend of the temperature evolution compared to MH-L and STD samples, suggesting a higher tendency for heat diffusion from the flame source towards the back side of the sample, compared to the MH-L flame retardant coating. However, a more accurate evaluation of the comparison between the various batches and of the extent of the flame-induced damage is believed to be productive to effectively evaluate the performance of the compared coatings.

In order to assess the effect of magnesium hydroxide and aluminum hydroxide on the flame-retardant behavior of acrylic based coating, the backside temperature reduction of the FR filled coatings, normalized to the coating thickness (X), compared to the STD one, and at increasing time during the fire retardant behavior tests performed at 30 s, are reported in Figure 4.

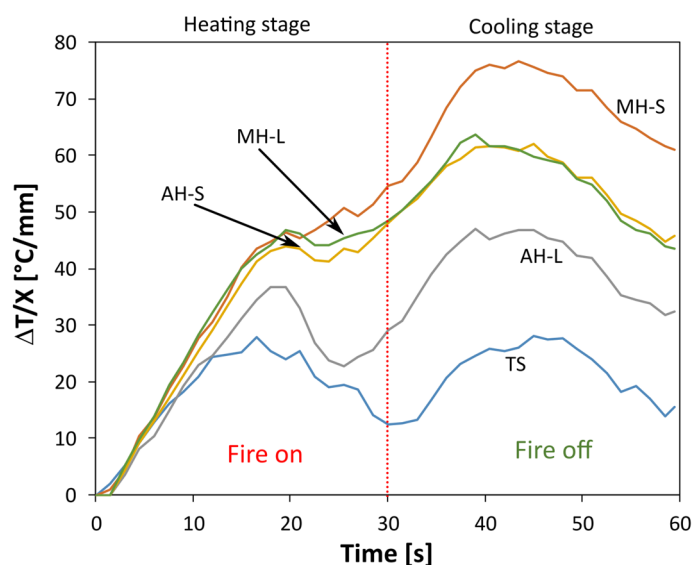


Figure 4. Difference in the back temperature variation (ΔT), normalized to the coating thickness (X), for all batches compared to the STD one during the direct impact flame (30 s).

The greater the $\Delta T/X$, the more effective the thermal barrier provided by the functional coating. The TS system (reference thermal protective coating) exhibits a bimodal trend, characterized by two very distinct peaks, occurring at approximately half of the heating and cooling cycle, respectively. The coating has a good protective action with a maximum $\Delta T/X$ equal to ~ 20 °C/mm. The addition of FR based on $\text{Al}(\text{OH})_3$ implies an improvement in thermal performance, with an evident increase in fire protection of the metal substrate. This effect is evident throughout the measurement range of the test. The maximum deviation with respect to the STD specimen is achieved during the cooling phase at approximately 45 s for the AH-S sample equal to 47.5 °C/mm.

The replacement of $\text{Al}(\text{OH})_3$ with $\text{Mg}(\text{OH})_2$ induces a further increase in performance. In particular, the MH-S specimen shows a monotonous and saddle-free trend at 30 s (usually induced by a burn-on/burn-off transition of the flame). This curve trend confirms the high

thermal stability of the functional coating. The limited degradation, even after long periods of exposure to direct flame, enhances the differences with respect to the other specimens.

It should be noted, in particular, that the specimens added with FR, characterized by a smaller particle size (MH-S and AH-S), have better fire protection properties. When the flame is removed (30 s), a further increase in temperature is recorded, due to thermal inertia, for up to 40 s. The other investigated batches do not show significantly different behavior from the TS one, in particular the AH-L specimen. A wider difference is found at longer exposure times. Large-sized particle fillers appear to require longer activation times to provide effective fire protection.

Analyzing the samples images after flame exposure (Figure 5), the STD batch displays the least effective fire-retardant performance, as demonstrated by the extensive carbonized area resulting, in particular, from 30 s of direct flame exposure. It is observable that the unfilled TS batch, used as a reference, displays a minor affected area during a brief exposure time. However, with longer exposure, there is no significant distinction between the TS batch and the AH-L 30 s batch.

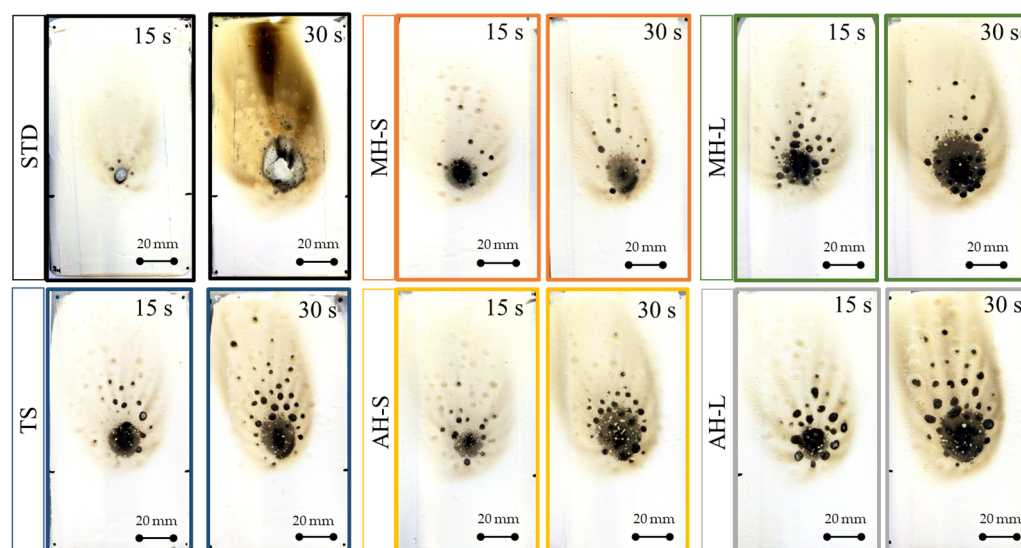


Figure 5. Fire test images of investigated samples.

Examining the specimens with the addition of hydroxides, it is noted that only the specimen which uses the fine-grained magnesium hydroxide has excellent fire stability. The area affected by the combustion appears more contained and relatively homogeneous. While aluminum hydroxide-based specimens exposed to fire for a longer time show worse performance, similar to the TS reference sample. This can be explained by the fact that during the dehydration process aluminum hydroxide absorbs less energy (1050 J/g) [1] than magnesium hydroxide (1389 J/g) [2]. The dehydration process is an endothermic process, which removes heat from the support, slowing down the thermal degradation of the coating and, in this case, releasing nontoxic and noncorrosive reaction products. However, according to Beyer et al. [1], $\text{Al}(\text{OH})_3$ triggers its protective function before $\text{Mg}(\text{OH})_2$, affecting the degradation at lower temperatures. The dehydration process of $\text{Mg}(\text{OH})_2$ occurs at higher temperatures, as well as its protective action. Therefore, the fire-retardant behavior becomes more relevant as the hydroxide dehydration temperature is approached.

After flame testing, the coatings reveal an area affected by combustion, consisting of three coded zones labeled as I, II, and III. Zone I represents the flame propagation region. Zone II indicates the area of contact between the flame and the paint and, as a result, it is the most darkened portion of the sample. Zone III is the white region where the flame did not propagate, and it closely resembles the fresh sample, i.e., the sample before conducting the tests. Figure 6 illustrates the three zones just described.

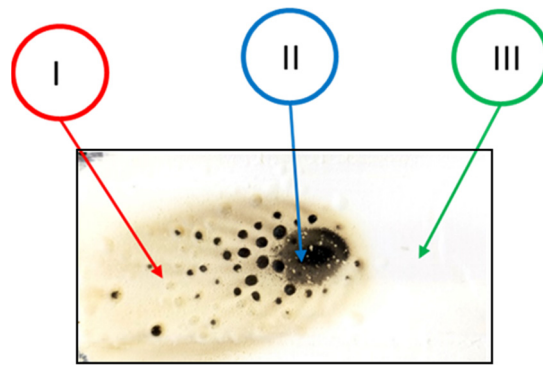


Figure 6. Coded zones of the coating area affected by the combustion.

Each zone was structurally characterized by X-Ray diffraction. A similar behavior was observed for all investigated coatings. For brevity, Figure 7 shows the diffractograms of TS and MH-S coatings, after exposure to the flame for 30 s. The diffractograms are compared to the fresh samples, not subjected to the flame test.

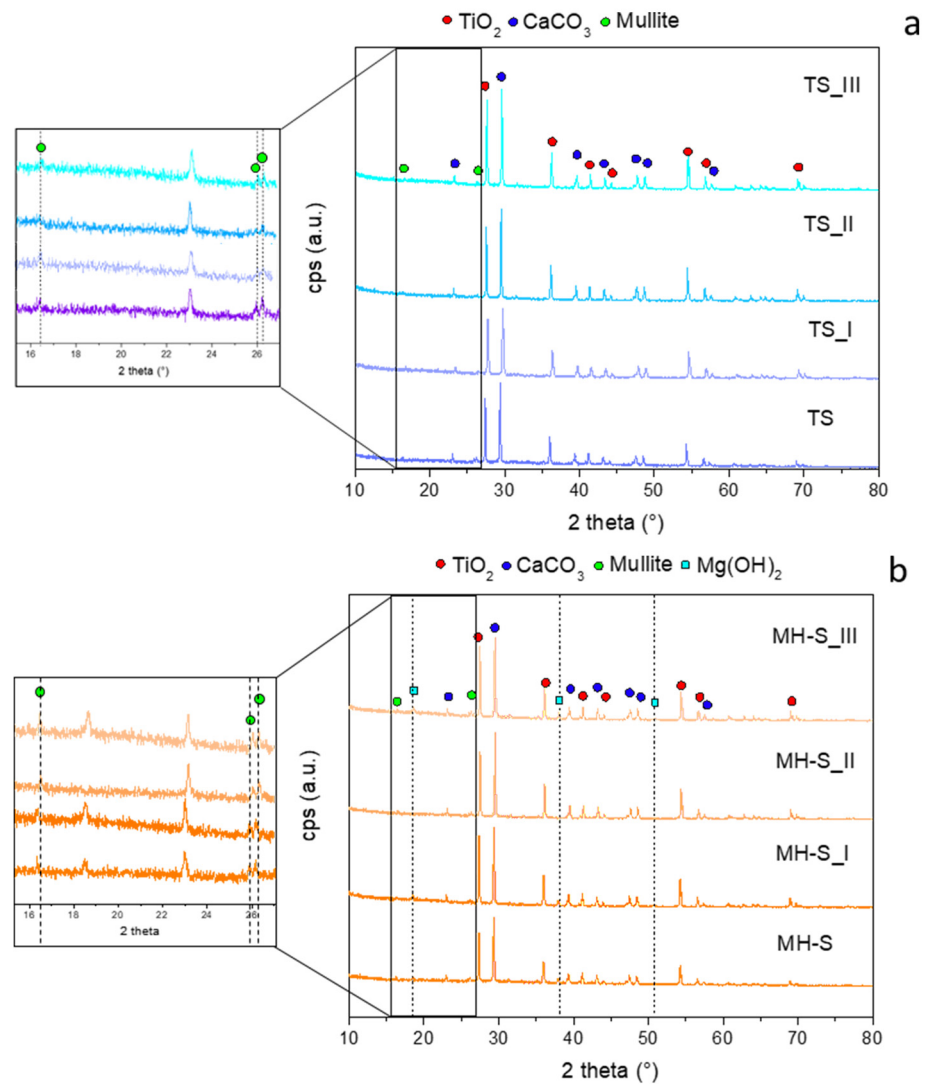


Figure 7. XRD images of TS (a) and MH-S (b) samples before and after flame test. Magnifications reveal the peaks of the mullite phase.

In Figure 7a, it is possible to observe that there are no structural differences between the sample before the fire test and the ones conducted on the three investigated zones after the flame experiment of the TS sample. All diffractograms show a clearly crystalline structure, mainly composed of two phases: TiO_2 (JCPDS #89-552) and CaCO_3 (JCPDS #1-83-1762). The less intense peaks of mullite (JCPDS #4-9-3667) are also noted.

However, in the case of the MH-S sample, Figure 7b shows a clear difference between the diffractogram of MH-S_II and the other ones. In fact, in this case, the brucite peaks (JCPDS #7-0239, 2theta: 18.6° , 38° , and 51°) disappear, resulting from its dehydration during the combustion of the coating.

In the diffractogram of Zone I, the aforementioned peaks are still clearly visible, probably because in this region the temperature did not exceed 300°C , which is necessary for the dehydration of $\text{Mg}(\text{OH})_2$.

Furthermore, it is interesting to note that the peaks related to periclase MgO (JCPDS #96-100-0054, 2theta: 36.86° , 42.8° , 62.19° , 74.43° , and 78.56°), formed during the dehydration reaction, are not clearly visible because they overlap with the more intense peaks of the standard vehicle. For both formulations, there are no evident differences concerning the mullite phase peaks (magnifications in Figure 7) in the three investigated zones in comparison with the samples before the flame exposure.

3.2. Digital Image Analysis

In order to better discriminate the evolution of the damage induced by the exposure of the coating to direct flame, the distribution of the degraded area was investigated by means of digital images analysis at varying exposure time and flame retardant in the coating. For the sake of brevity, Figure 8 shows the discretization results, obtained by digital image analysis, for a reference AH-L coating at varying exposure time to direct flame. The same discretization approach was applied for all investigated batches.

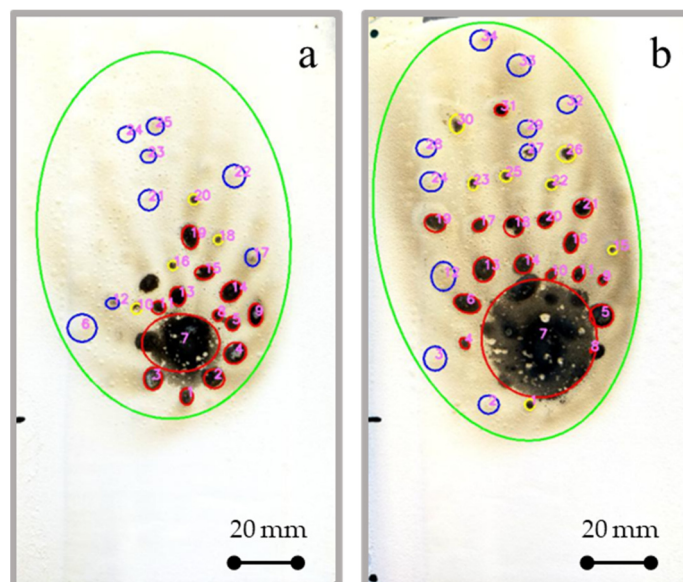


Figure 8. Discretization by digital image analysis of fire damage events in AH-L sample exposed for (a) 15 s and (b) 30 s to direct flame.

The algorithm has been tailored to discriminate the area that has undergone the direct exposure to fire (central area highlighted with a large red circle in Figure 8). In addition, a wide and very large area (green circle in Figure 8) was distinguished. It identifies the zone of the coating that was affected by the severe local heat treatment. Similarly, various degradation phenomena have been distinguished within this large area.

At first, it was possible to identify with good approximation the local carbonization events which occurred randomly in the neighboring area of the flame contact zone (small

red circles in Figure 8). This area, having been strongly affected by the thermal source, underwent a rise in temperature, which led to the degradation of the low melting materials. The consequence is the formation of small carbonaceous and randomly dispersed dimples that follow the heat flow induced by the flame. These can be due to the charring of local regions characterized by a high concentration of acrylic matrix [25].

Furthermore, in the area far from the fire exposition, local degradation events have been distinguished, in which there is an evident browning of the surface (small blue circles in Figure 8). In this area, the reached temperature is considerably lower than in the red zone, thus not inducing the pyrolysis of their constituents. However, a broad and diffuse surface oxidation process of the sample is triggered. Finally, in the transition zone between the soft (blue cycles) and the hard (red circles) heated zone, some very small black degraded dimples (yellow cycles) are observed.

Based on the applied discretization process, an analysis of the frequency distribution of the fire-induced defect areas was conducted. Figure 9 shows the frequency plot in AH-L samples exposed for 15 s and 30 s to direct flame. The AH-L-15 sample exhibits a single cluster of defects with an intermediate area ($\sim 12.5\text{--}22.5\text{ mm}^2$), due to a partial activation of fire-induced degradation phenomena. Instead, the AH-L-30 sample, exposed for 30 s to direct flame, is characterized by two well-defined peaks at low and high dimension. The former peak, with a maximum at 7.2 mm^2 , can be related to the formation of new degraded nuclei, which extend further away from the flame zone. The second peak correlated to greater area defects (the maximum of the peak at about 21.1 mm^2) is instead attributable to the growth of the defects colony observed at the end of the 15 s exposure test.

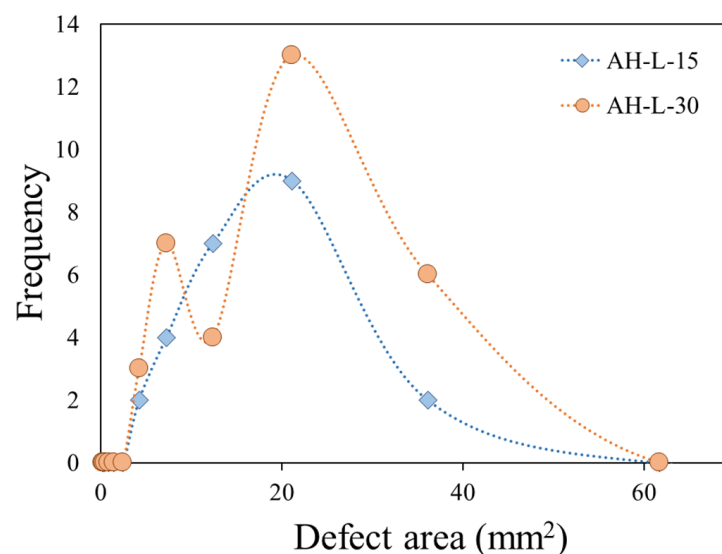


Figure 9. Frequency plot of fire-induced defect area distribution in AH-L sample exposed for 15 s and 30 s to direct flame.

Similar results, with evidence of a bimodal trend in the distribution of the defect areas with a long exposure time to fire, were found for all the investigated batches. Obviously, the size of the defect areas in correspondence with the peak varied according to the greater or lesser tendency to deteriorate, during the direct exposure to fire. In this concern, for clarity, Figure 10 compares the frequency distribution (expressed in percentage to facilitate the comparison among all batches) of the flame-induced defect area for all samples exposed for 15 s and 30 s to direct flame. In order to increase the plot readability, the defect area axis was defined in log scale.

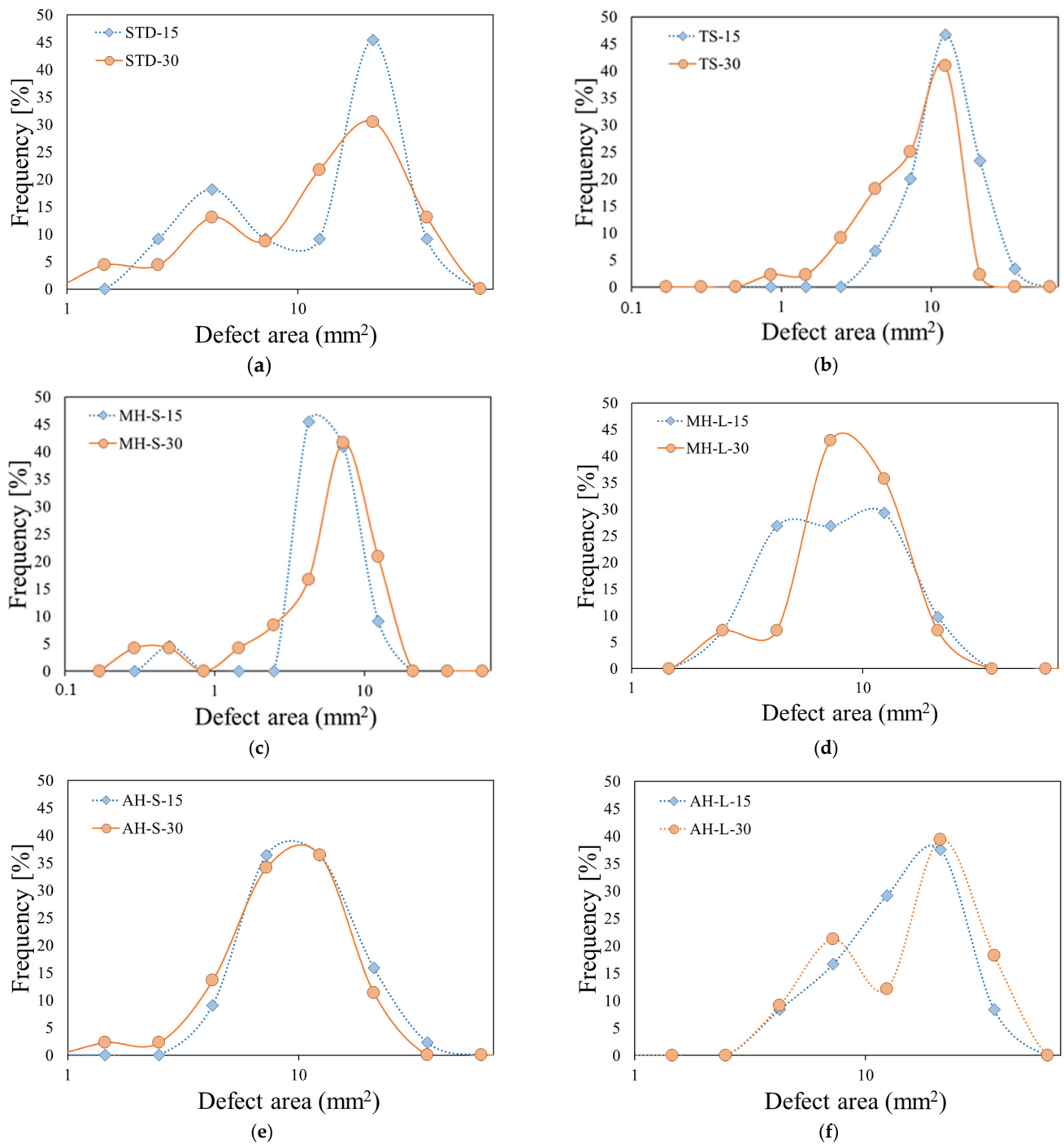


Figure 10. Frequency percentage plot of flame-induced defect area distribution for all samples exposed for 15 s and 30 s to direct flame. (a) STD; (b) TS; (c) MH-S; (d) MH-L; (e) AH-S; (f) AH-L.

3.3. Fire Damage Maps

Based on the previous consideration, in all coated samples, the flame-induced damage can be discriminated into four zones:

- FCZ. Fire Carbonized Zone. It is the area directly exposed to the flame. The coating reaches high temperatures undergoing pyrolysis. It is easily identified by the black carbonaceous surface obtained at the end of the test.
- FDZ. Fire Dimpled Zone. It is the area near the flame exposure area. Fire-induced degradation is relevant, and its morphology is characterized by colonies of dark dimples.

- TZ. Transition zone. Progressively increasing the distance from the flame exposition area, the effect is gradually less relevant. In this zone, the dimples do not become carbonaceous. Although, a local, circular shaped browning is detected, indicating that the degradation phenomenon has been activated but sufficient temperatures have not been reached to activate local pyrolysis.
- HAZ. Heat affected zone. This region suffers a limited modification induced by the flame test, showing, in particular, a slight superficial browning.
- N-HAZ. Not Heat affected zone. This region does not suffer thermal effects induced by the flame test. No surface modifications are observed.

Figure 11 shows, as reference, the fire damage zones occurring by varying the exposure time to direct flame for the AH-L coating batch.

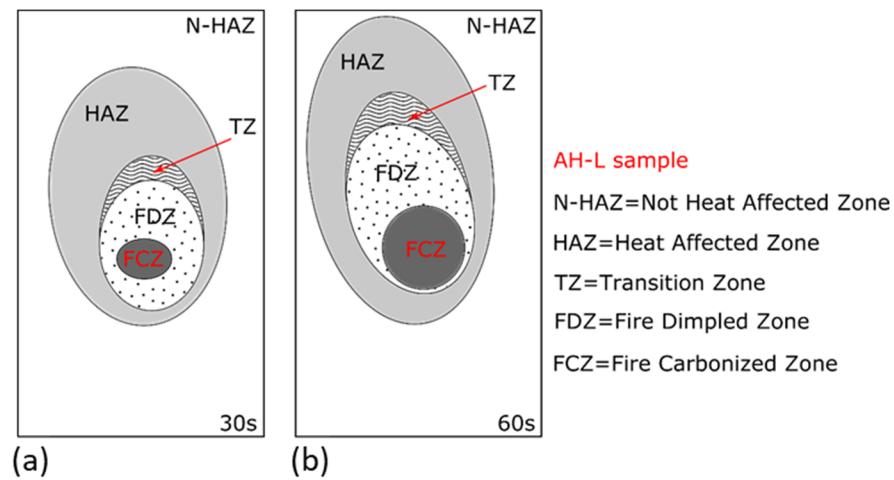


Figure 11. Scheme of evolution of fire damage zones for (a) AH-L-15 and (b) AH-L-30 samples.

Increasing the time of exposure to fire increases the degradation areas that can be identified. In particular, the heat-affected zone extends for a large part of the surface, confirming the severe thermal treatment imposed by the direct flame exposition (e.g., increase in HAZ and FCZ areas). Interesting considerations can be argued by comparing the extent of these areas as a function of the fire-retardant compound used in the composite coating.

Figure 12 shows the area of FDZ (fire dimpled zone, expressed in cm²) for all batches exposed for 15 s and 30 s to direct flame.

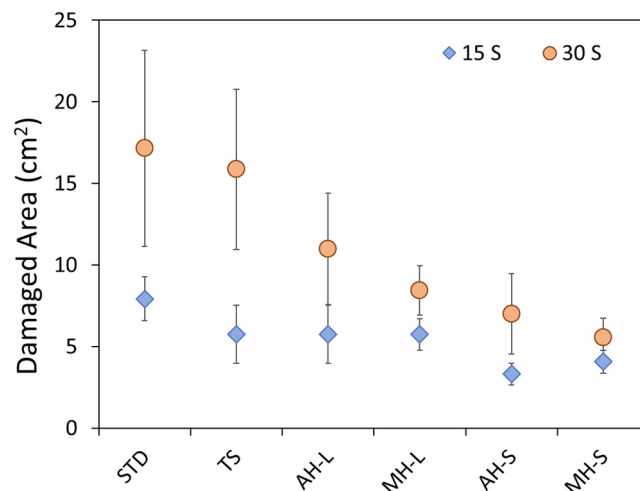


Figure 12. Area of FDZ damage zone for all batches exposed for 15 s and 30 s to direct flame.

As attended, the STD batch exhibits the worst fire-retardant behavior, as evidenced by the large FDZ area that after 30 s of exposition to direct flame reached a value of $\sim 17.2 \text{ cm}^2$. This indicates that a large carbonization area along the flame direction occurred, indicating that the protective capacity supplied by this reference batch is not effective. The addition of thermos-active fillers can offer a clear increase in flame stability and improve the protection of the coating in severe thermal conditions (e.g., direct contact with fire).

It can be noted that the unmodified reference TS batch shows a small FDZ damaged area at low exposition time. At high exposition time, the results are almost compatible with the STD one. This implies that the TS specimen shows adequate fire-retardant behavior only at low exposure times. Its protective efficacy is significantly reduced for longer exposure times. Conversely, there is a significant reduction in the damaged area, even at long exposure times, for the modified coatings. Magnesium hydroxide appears to show better efficacy than aluminum hydroxide. Furthermore, low grain size fire-retardant compounds exhibit the most satisfactory results. Best results were observed for the MH-S batch, where an FDZ damage area equal to 4.1 cm^2 and 5.6 cm^2 was observed for 15 s and 30 s of exposition to direct flame, respectively.

The aluminum hydroxide modified coatings (AH-L and AH-S batches) evidenced a slightly larger damaged area than corresponding magnesium hydroxide modified coatings. The hydroxides influence the thermal degradation of the modified coating in a temperature range strictly related to the dehydration process of each hydroxide. In particular, the decomposition reaction of $\text{Al}(\text{OH})_3$ takes place in a temperature range of $180\text{--}230 \text{ }^\circ\text{C}$ [26,27]. Instead, the dehydration reaction of $\text{Mg}(\text{OH})_2$ occurs at about $200\text{--}400 \text{ }^\circ\text{C}$ [28]. Considering the temperatures reached by the specimen during the fire test, this latter offers a better flame-retardant capacity providing a suitable thermal degradation barrier.

With the aim of having a further assessment of the fire-retardant behavior of the different modified coatings, Figure 13 compares all areas of damage zones for all batches exposed for 15 s and 30 s to direct flame. The results show that the HAZ area does not have a clear dependence on the modification coating. There is a slight decrease in the average value of HAZ area due to the addition of the fire-resistant compound and choosing a fine particle size of it. However, the dispersion of the results is such that this trend is not statistically significant. Different considerations can be drawn by analyzing the other zones (FCZ, FDZ, TZ), for which there is an evident reduction in the damage area induced by the flame test following the modification of the coating. Especially for the areas near the flame, e.g., FCZ and FDZ, it is evidenced that the fire-retardant protective action has a marked effect. The selection of a proper fire-retardant compound has a key role in the fire protection of the coating. The MH-S-30 specimen shows a reduction in the FCZ and FDZ areas of 53% and 65%, compared to the TS-30 specimen (identified as unmodified reference fire resistant batch). These results suggest the clear shielding action to heat diffusion induced by the fire-resistant compound addition. In particular, a better thermal barrier effect is noted for the system based on $\text{Mg}(\text{OH})_2$ compared to the $\text{Al}(\text{OH})_3$ formulations.

Magnesium and aluminum hydroxides play a relevant role in the thermal energy dissipation during the fire test. According to reaction (1) and reaction (2) both of them, due to the endothermic dehydration reaction, decompose in oxides and water vapor [7,26]. However, the incipient decomposition temperature of the dehydration process and the related enthalpy of endothermic reaction is different for the two oxides. $\text{Mg}(\text{OH})_2$ dehydrates at $332 \text{ }^\circ\text{C}$, about $150 \text{ }^\circ\text{C}$ higher than $\text{Al}(\text{OH})_3$ filler (that dehydrates at $180 \text{ }^\circ\text{C}$) involving, furthermore, an enthalpy of 1389 J/g [8], despite the $\text{Al}(\text{OH})_3$ being characterized by 1050 J/g [9].

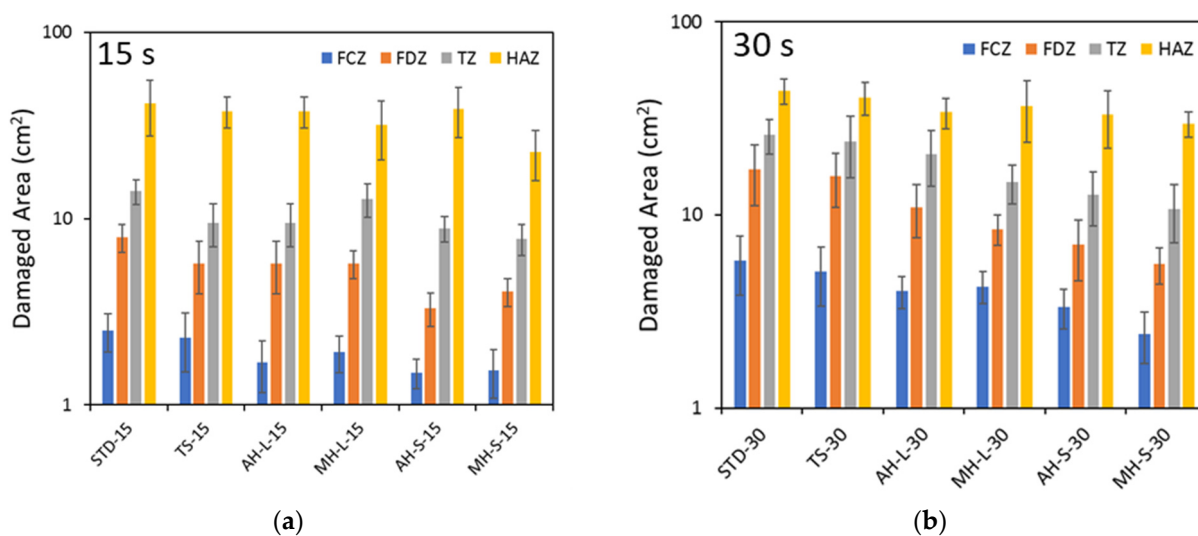


Figure 13. Area of damage zones for all batches exposed for (a) 15 s and (b) 30 s to direct flame.

In summary, it can be highlighted that the coatings modified with fine-grained compounds (MH-S and AH-S) evidenced a more effective fire protection than the complementary large-grained ones (MH-L and AH-L), as identifiable by the areas of damage observed for these batches. This behavior could be related considering that a small particle size favors a suitable distribution of the thermal active filler thus exalting the thermal exchange and fire-retardant capacity of the coatings. Furthermore, a lower activation time required by the fine-grained additives, compared to the coarse-grained ones, triggers an effective fire protection thus providing a more effective fire-retardant capacity for this class of coatings [29].

Magnesium (Mg) and Aluminum (Al) hydroxides have proven to be highly effective as fireproof coatings due to their chemical structure and composition. These materials provide a high level of resistance to burns and their thermal decomposition process effectively prevents ignition of the metal substrate. Additionally, their flame-retardant effect is highly homogeneous and efficient when the surface area is large, which is achieved through the use of small particle sizes. Practical engineering applications will depend on addressing challenges related to compatibility with different base vehicles, mechanical properties, and application techniques. With ongoing research and development, these additives could find increasing promotion prospects in the field of fire-resistant coatings. The results of the study have been highly promising, particularly in the case of the MH-S batch. This type of coating could serve as a long-term protection mechanism against accidental fire hazards, making it highly efficient in fire protection.

4. Conclusions

Four formulations of flame-retardant coatings were analyzed in this work. The used fillers were harmless $Mg(OH)_2$ and $Al(OH)_3$. All the coatings were tested, after being spread on a metal support, using an experimental set-up, capable of monitoring the surface in contact with the flame and the insulating properties of the coatings, by means of a thermocouple placed on the back of the sample under investigation. Comparing the coatings with an unfilled reference specimen, an improvement in the flame-retardant properties of the modified samples was evidenced. The samples added with hydroxide fillers demonstrated greater flame stability and better thermal insulation (calculated using the temperature measured by a thermocouple on the back side of the sample). Two sizes of filler particles were investigated. The sample coated with a nonflame-retardant paint reached a maximum back temperature of $129.5\text{ }^\circ\text{C}$, while AH-L (large $Al(OH)_3$ particle filled coating) showed a maximum temperature of $91.8\text{ }^\circ\text{C}$. Furthermore, through a process of digital image analysis (DIA), it was possible to examine the area damaged by the

combustion process. The best results were observed for the MH-S batch, where an FDZ damage area equal to 4.1 cm² and 5.6 cm² was observed for 15 s and 30 s exposure to direct flame, especially MH-S-30 which showed a 65% smaller area than the unmodified flame-retardant reference sample (TS-30).

Author Contributions: Conceptualization, E.P. (Edoardo Proverbio); data curation, L.C.; formal analysis, G.S., E.P. (Elpida Piperopoulos) and L.C.; Funding acquisition, M.A. and E.P. (Edoardo Proverbio); methodology, G.S. and E.P. (Elpida Piperopoulos); project administration, E.P. (Edoardo Proverbio); resources, M.A. and E.P. (Edoardo Proverbio); supervision, E.P. (Edoardo Proverbio); validation, E.P. (Elpida Piperopoulos) and L.C.; Writing—original draft, E.P. (Elpida Piperopoulos) and L.C.; writing—review and editing, G.S. All authors have read and agreed to the published version of the manuscript.

Funding: This research was funded by PON “Ricerca e Innovazione 2014 e 2020” and FSC, Project ARS01_00293 THALASSA—Technology and materials for safe Low consumption and low life cycle cost vessels and crafts, CUP B46C18000720005. Proposing party: Distretto NAVTEC.

Institutional Review Board Statement: Not applicable.

Informed Consent Statement: Not applicable.

Data Availability Statement: The data presented in this study are available on request from the corresponding author.

Conflicts of Interest: The authors declare no conflict of interest.

References

1. Mohd Sabee, M.M.; Itam, Z.; Beddu, S.; Zahari, N.M.; Mohd Kamal, N.L.; Mohamad, D.; Zulkepli, N.A.; Shafiq, M.D.; Abdul Hamid, Z.A. Flame Retardant Coatings: Additives, Binders, and Fillers. *Polymers* **2022**, *14*, 2911. [[CrossRef](#)]
2. Chen, H.; Zhou, J.; Liu, S.; Wang, S.; Gong, X. A Novel Anti-Impact and Flame Retardant Gel towards Human Protection and High-Temperature Alarm. *Compos. Part A Appl. Sci. Manuf.* **2022**, *158*, 106994. [[CrossRef](#)]
3. Wen, O.Y.; Tohir, M.Z.M.; Yeaw, T.C.S.; Razak, M.A.; Zainuddin, H.S.; Hamid, M.R.A. Fire-Resistant and Flame-Retardant Surface Finishing of Polymers and Textiles: A State-of-the-Art Review. *Prog. Org. Coat.* **2023**, *175*, 107330. [[CrossRef](#)]
4. Li, F.-F. Comprehensive Review of Recent Research Advances on Flame-Retardant Coatings for Building Materials: Chemical Ingredients, Micromorphology, and Processing Techniques. *Molecules* **2023**, *28*, 1842. [[CrossRef](#)] [[PubMed](#)]
5. Kablov, V.F.; Novopoltseva, O.M.; Kochetkov, V.G.; Lapina, A.G.; Pudovkin, V.V. Elastomer Heat-Shielding Materials Containing Aluminosilicate Microspheres. *Russ. Eng. Res.* **2017**, *37*, 1059–1061. [[CrossRef](#)]
6. Alonso, C.; Manich, A.; Campo, A.D.; Felix-De Castro, P.; Boisseree, N.; Coderch, L.; Martí, M. Graphite Flame Retardant Applied on Polyester Textiles: Flammable, Thermal and in Vitro Toxicological Analysis. *J. Ind. Text.* **2022**, *51*, 4424S–4440S. [[CrossRef](#)]
7. Brostow, W.; Lohse, S.; Lu, X.; Osmanson, A.T. Nano-Al(OH)₃ and Mg(OH)₂ as Flame Retardants for Polypropylene Used on Wires and Cables. *Emerg. Mater.* **2019**, *2*, 23–34. [[CrossRef](#)]
8. Günter Beyer, C.H. *Reactive Extrusion: Principles and Applications*; Wiley VCH: Weinheim, Germany, 2018.
9. Piperopoulos, E.; Mastronardo, E.; Fazio, M.; Lanza, M.; Galvagno, S.; Milone, C. Synthetic Strategies for the Enhancement of Mg(OH)₂ Thermochemical Performances as Heat Storage Material. *Energy Procedia* **2018**, *155*, 269–279. [[CrossRef](#)]
10. Miyata, S.; Imahashi, T.; Anabuki, H. Fire-Retarding Polypropylene with Magnesium Hydroxide. *J. Appl. Polym. Sci.* **1980**, *25*, 415–425. [[CrossRef](#)]
11. Peng, H.-K.; Wang, X.; Li, T.-T.; Lou, C.-W.; Wang, Y.; Lin, J.-H. Mechanical Properties, Thermal Stability, Sound Absorption, and Flame Retardancy of Rigid PU Foam Composites Containing a Fire-Retarding Agent: Effect of Magnesium Hydroxide and Aluminum Hydroxide. *Polym. Adv. Technol.* **2019**, *30*, 2045–2055. [[CrossRef](#)]
12. Córdova-Suárez, M.; Barreno-Avila, E.M.; Pozo-Álvarez, D.S.; Córdova-Suárez, J.C. Inorganic Flame Retardants’ Efficacy of Aluminum Hydroxide, Magnesium Hydroxide in the Combustion Rate of Intermediate Calamagrostis from Ecuador’ Moorlands. *IOP Conf. Ser. Mater. Sci. Eng.* **2021**, *1173*, 12070. [[CrossRef](#)]
13. Yew, M.C.; Ramli Sulong, N.H.; Yew, M.K.; Amalina, M.A.; Johan, M.R. Influences of Flame-Retardant Fillers on Fire Protection and Mechanical Properties of Intumescent Coatings. *Prog. Org. Coat.* **2015**, *78*, 59–66. [[CrossRef](#)]
14. Liang, J.; Zhang, Y. A Study of the Flame-Retardant Properties of Polypropylene/Al(OH)₃/Mg(OH)₂ Composites. *Polym. Int.* **2010**, *59*, 539–542. [[CrossRef](#)]
15. Liang, J.Z.; Chen, Y.; Jiang, X.H. Flame-Retardant Properties of PP/Al(OH)₃/Mg(OH)₂/POE/ZB Nanocomposites. *Polym. Plast. Technol. Eng.* **2012**, *51*, 439–445. [[CrossRef](#)]
16. Cheng, L.; Ren, S.; Brosse, N.; Ju, Z.; Li, S.; Lu, X. Synergic Flame-Retardant Effect of Cellulose Nanocrystals and Magnesium Hydroxide in Polyurethane Wood Coating. *J. Wood Chem. Technol.* **2022**, *42*, 297–304. [[CrossRef](#)]

17. Chen, H.; Wen, X.; Guan, Y.; Min, J.; Wen, Y.; Yang, H.; Chen, X.; Li, Y.; Yang, X.; Tang, T. Effect of Particle Size on the Flame Retardancy of Poly(Butylene Succinate)/Mg(OH)₂ Composites. *Fire Mater.* **2016**, *40*, 1090–1096. [[CrossRef](#)]
18. Liang, J.Z.; Feng, J.Q.; Tsui, C.P.; Tang, C.Y.; Liu, D.F.; Zhang, S.D.; Huang, W.F. Mechanical Properties and Flame-Retardant of PP/MRP/Mg(OH)₂/Al(OH)₃ Composites. *Compos. Part B Eng.* **2015**, *71*, 74–81. [[CrossRef](#)]
19. Mastronardo, E.; Kato, Y.; Bonaccorsi, L.; Piperopoulos, E.; Milone, C. Thermochemical Storage of Middle Temperature Wasted Heat by Functionalized C/Mg(OH)₂ Hybrid Materials. *Energies* **2017**, *10*, 70. [[CrossRef](#)]
20. Lam, Y.L.; Kan, C.W.; Yuen, C.W.M. Effect of Titanium Dioxide on the Flame-Retardant Finishing of Cotton Fabric. *J. Appl. Polym. Sci.* **2011**, *121*, 267–278. [[CrossRef](#)]
21. Ersoy, O.; Fidan, S.; Köse, H.; Güler, D.; Özdöver, Ö. Effect of Calcium Carbonate Particle Size on the Scratch Resistance of Rapid Alkyd-Based Wood Coatings. *Coatings* **2021**, *11*, 340. [[CrossRef](#)]
22. Berman, A.; DiLoreto, E.; Moon, R.J.; Kalaitzidou, K. Hollow Glass Spheres in Sheet Molding Compound Composites: Limitations and Potential. *Polym. Compos.* **2021**, *42*, 1279–1291. [[CrossRef](#)]
23. Catarina, G.A.S.; Borsoi, C.; Romanzini, D.; Piazza, D.; Kunst, S.R.; Scienza, L.C.; Zattera, A.J. Development of Acrylic-Based Powder Coatings with Incorporation of Montmorillonite Clays. *J. Appl. Polym. Sci.* **2017**, *134*, 45031. [[CrossRef](#)]
24. Sturges, H.A. The Choice of a Class Interval. *J. Am. Stat. Assoc.* **1926**, *21*, 65–66. [[CrossRef](#)]
25. El Hage, R.; Viretto, A.; Sonnier, R.; Ferry, L.; Lopez-Cuesta, J.-M. Flame Retardancy of Ethylene Vinyl Acetate (EVA) Using New Aluminum-Based Fillers. *Polym. Degrad. Stab.* **2014**, *108*, 56–67. [[CrossRef](#)]
26. Elbasuney, S. Novel Multi-Component Flame Retardant System Based on Nanoscopic Aluminium-Trihydroxide (ATH). *Powder Technol.* **2017**, *305*, 538–545. [[CrossRef](#)]
27. Živković, Ž.D.; Dobovišek, B. Kinetics of Aluminium Hydroxide Dehydration. *J. Therm. Anal. Calorim.* **2005**, *12*, 207–215. [[CrossRef](#)]
28. Mastronardo, E.; Bonaccorsi, L.; Kato, Y.; Piperopoulos, E.; Milone, C. Efficiency Improvement of Heat Storage Materials for MgO/H₂O/Mg(OH)₂ Chemical Heat Pumps. *Appl. Energy* **2016**, *162*, 31–39. [[CrossRef](#)]
29. Piperopoulos, E.; Scionti, G.; Atria, M.; Calabrese, L.; Proverbio, E. Flame-Retardant Performance Evaluation of Functional Coatings Filled with Mg(OH)₂ and Al(OH)₃. *Polymers* **2022**, *14*, 372. [[CrossRef](#)]

Disclaimer/Publisher’s Note: The statements, opinions and data contained in all publications are solely those of the individual author(s) and contributor(s) and not of MDPI and/or the editor(s). MDPI and/or the editor(s) disclaim responsibility for any injury to people or property resulting from any ideas, methods, instructions or products referred to in the content.